Available online at www.sciencedirect.com
SCIENCE DIRECT®
C. R. Physique 4 (2003) 265–274
COMPTES RENDUS PHYSIQUE

Hydrodynamics and physics of soft objects/Hydrodynamique et physique des objets mous

Dynamic strength of fluid membranes

Force dynamique des membranes fluides

Evan Evans [a,b,*], Volkmar Heinrich [b]

[a] *Departments of Physics and Pathology, University of British Columbia, Vancouver V6T 1Z1, BC, Canada*
[b] *Departments of Biomedical Engineering and Physics, Boston University, Boston, MA 02215, USA*

Presented by Guy Laval

Abstract

Rupturing fluid membrane vesicles with a steady ramp of micropipette suction yields a tension distribution that images the kinetic process of membrane failure. When plotted on a log scale of tension loading rate, the distribution peaks (membrane strengths) define a *dynamic tension spectrum* with distinct regimes that reflect passage of prominent energy barriers along the pathway to rupture. Demonstrated here by tests on giant PC lipid vesicles over loading rates from 0.06–60 mN/m/s, the stochastic process of rupture can be modelled as a causal sequence of two thermally-activated transitions where each transition governs membrane strength on separate scales of loading rate. Under fast ramps of tension, a steep linear regime appears in each spectrum at high strengths which implies that failure requires nucleation of a rare nanoscale defect. The slope and projected intercept yield defect size and spontaneous production rate respectively. However, under slow ramps of loading, the spectrum crosses over to a shallow-curved regime at lower strength, which is consistent with the kinetic impedance to opening an unstable hole in a fluid film. The dependence of rupture tension on rate reveals hole edge energy and frequency scale for thermal fluctuations in size. ***To cite this article: E. Evans, V. Heinrich, C. R. Physique 4 (2003).***

Résumé

La rupture de vésicules membranaires fluides sous différentes rampes de succion appliquées à l'aide de micropipettes génère des distributions de tension qui révèlent un processus cinétique de rupture membranaire. Le spectre dynamique exprimant *la tension de rupture* en fonction de la vitesse de succion (*taux de charge*) en échelle logarithmique met en évidence les barrières d'énergie qui empêchent la rupture et limitent la perméation spontanée. Les expériences réalisées sur des vésicules lipidiques géantes pour des taux de charge de 0,06–60 mN/m/s montrent que la résistance de la membrane est gouvernée par deux transitions thermiquement activées. Pour les résistances les plus élevées sous des vitesses de succion rapides, un régime linéaire dans le spectre est dominé par une nucléation initiale de défauts à une échelle nanoscopique. La pente et l'intersection avec l'axe des abscisses permettent de déduire respectivement de la taille du défaut et de la vitesse spontanée. A de plus faibles tensions de rupture sous de faibles taux de charge, un régime de faible courbure dans le spectre est dominé par le processus mésoscopique d'ouverture d'un pore pour lequel l'échelle des tensions révèle une énergie de ligne. ***Pour citer cet article : E. Evans, V. Heinrich, C. R. Physique 4 (2003).***

Keywords: Membrane rupture and permeation; Edge energy-line tension; Dynamic tension spectroscopy

Mots-clés : Rupture et perméation des membranes ; Barrière d'énergie-tension de rupture ; Spectroscopie de la tension dynamique

* Corresponding author.
E-mail address: evans@physics.ubc.ca (E. Evans).

1631-0705/03/$ – see front matter
doi:10.1016/S1631-0705(03)00044-6

1. Introduction

Unstressed, a fluid membrane in the form of a closed vesicle or solid supported film can survive for a very long period of time. However, under lateral stress, membrane tension will reach a level where a nanoscale hole opens and grows rapidly to rupture the membrane. The question is: what governs the level of tension needed for failure and thus determines membrane strength? Held together by hydrophobic interactions, one might naively expect fluid lipid bilayers to rupture at tensions comparable to hydrocarbon-water surface tension ($\sigma_{o/w} \sim 40$ mN/m) by analogy to when surface pressure vanishes in a lipid monolayer spread at an oil/water boundary. However, biomembranes rupture at much lower tensions in a range from ∼1–25 mN/m and exhibit a prominent dependence on lipid composition [1–6]. Although commonly considered as material *constants*, we will show that rupture strengths of fluid membranes are dynamical properties and depend on the time frame for breakage.

Many clever experiments have been designed to observe transient permeation and opening of membrane holes. In the majority of experiments, holes in membranes have been produced in planar films under constant lateral tension using transmembrane voltages often sufficient to cause capacitive breakdown [7–13]. More recently, holes in vesicle membranes have been opened by adhesion-driven tension and slowed through viscous thickening of the aqueous environment to enable observation by video microscopy [14,15]. Complementary to these techniques, but linked in a more direct way to the determinants of mechanical strength, we will show that rupturing vesicle or cell membranes under ramps of tension in time ($\sigma = \Re_\sigma t$) provides a simple mechanical method to explore the kinetic process of hole nucleation and dynamics of membrane failure. If performed over a sufficient span in loading rate $\Re_\sigma$, measurements of rupture tension versus $\log(\Re_\sigma)$ can reveal the dominant nano-to-mesoscale energy barriers traversed along the tension-driven pathway to membrane failure. Here, we demonstrate the approach with results from tests on giant phosphatidyl choline PC vesicles loaded at rates over nearly four orders of magnitude in tension/time. The dependence of breakage tension on rate implies a kinetic process that begins with nucleation of a nanoscale defect which then either vanishes or evolves to an unstable hole. Correlation of the measured statistics of failure to distributions predicted by the theory yields the size and frequency of formation for the initial defect plus the attempt rate and hole edge energy that govern passage of the final barrier to catastrophic failure.

2. Materials and methods

2.1. Lipids and vesicle preparation

Fluid membrane vesicles were made from *cis* unsaturated 1-stearoyl-2-oleoyl-sn-glycero-3-phosphocholine (C18:0/1)-SOPC, 1,2-dioleoyl-sn-glycero-3-phosphocholine (diC18:1) DOPC, and 1,2-dilinoleoyl-sn-glycero-3-phosphocholine (diC18:2) DLnOPC. These synthetic species of diacyl PC lipids were purchased from Avanti Polar Lipids (Alabaster, AL) in chloroform and used without further purification. The solutions were stored in amber glass screw cap vials with Teflon-lined silicone septa, wrapped in aluminum foil, and kept at −20 °C under argon. To create giant bilayer vesicles (15–40 μm diameter), lipid films were first dried from chloroform:methanol (2:1) onto the surface of a roughened Teflon disk [16]. After deposition of the lipid film and evaporation of the organic solvent in vacuo, the Teflon disk was covered with a film of warm (37 °C) sucrose solution (200 mM) and allowed to pre-hydrate before swelling in excess buffer. The final aliquot of giant vesicles was produced by many-fold dilution of the hydrated lipid multilayers in an equi-osmolar glucose or salt buffer. The difference in inner and outer solutes creates both a refractive index and density gradient, which enhance optical discrimination of the vesicle contour (cf. Fig. 1) and sediment vesicles to the floor of the microscope chamber.

2.2. Measurement of rupture strength

Micropipet pressurization was used to increase membrane tension and lyse single vesicles. To increase tension at a steady rate, a ramp of pipet suction $P(t) = c_p t$ was produced with a motorized ground-glass syringe pump connected to the micropipet assembly. Tension was calculated from the pressure using the well-known relation for a fluid membrane vesicle [17], $\sigma(t) = P(t)R_p/2(1 - R_p/R_s)$. In addition to the pre-measured value of inner pipet radius R_p, the radius R_s of the vesicle exterior to the pipet was monitored continuously throughout each test. The loading rate $\Re_\sigma$ was determined directly from the slopes of tension versus time. High speed video-image analysis was used to track vesicle boundaries along the axis of symmetry at a framing rate of $\sim 100\ s^{-1}$. Samples of intensity profiles prior to – and just after – rupture are shown in Fig. 1. Vesicle rupture led to disappearance of the vesicle within 1–2 image frames and accurately defined rupture tension within $0.01\Re_\sigma$ (mN/m). Optical measurement of pipette radius contributed a random uncertainty of $\sim \pm 5\%$ to the magnitude of tension and tension loading rate.

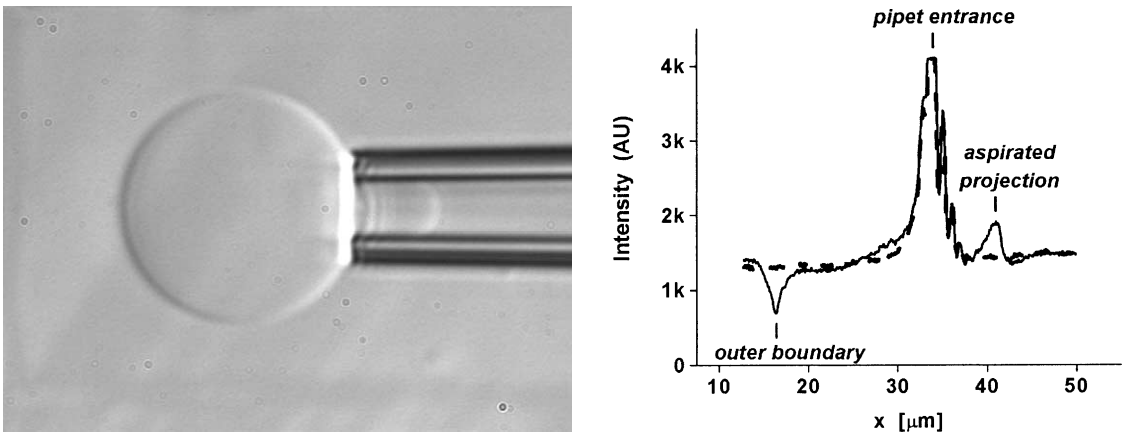

Fig. 1. Left: video image of a giant PC bilayer vesicle aspirated into a micropipette; right: intensity scans along the axis of symmetry before (solid curve) and after vesicle rupture (dotted curve).

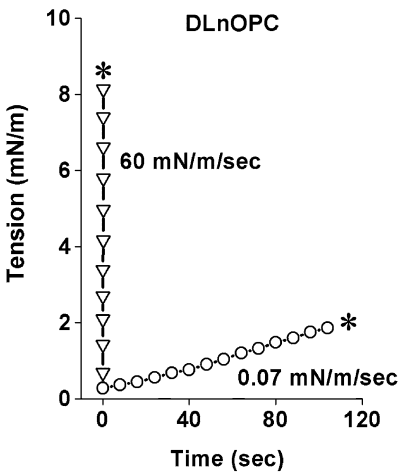

Fig. 2. Membrane tension as function of time for two vesicles made from diC18:2 PC and loaded at slow and fast loading rates up to rupture (stars).

2.3. Experimental results

Fig. 2 shows tension histories for two vesicles tested under a slow and fast loading rate. Made with the same type of lipid, the major increase in rupture tension at the fast rate compared to the slow rate demonstrates the underlying dependence of membrane rupture on kinetics. Performed at 6 loading rates in the range from 0.06–60 mN/m/s, histograms of rupture tensions were collected from lysis of 70–100 vesicles at each rate. The evolution in statistics of rupture events from the slowest to fastest loading rates are demonstrated by the sample histograms for each type of lipid in Fig. 3. Superposed on the histograms are probability densities for failure predicted by the kinetic theory for rupture, which will be developed in the following section. Readily apparent in Fig. 3, the positions of histograms shift to higher tensions as loading rate increases. Secondly, the shapes of distributions begin narrow at slow rates and broaden asymmetrically on approach to fast rates. Also, the spreads in rupture tension are significantly greater than that contributed by experimental error at all loading rates. From the viewpoint of material properties, the level of membrane rupture strength is seen to diminish with increased lipid unsaturation at a fixed chain length. As we will show next, the parameters needed to predict the rupture statistics at any loading rate are readily obtained from analysis of the dynamic spectra of most frequent rupture tensions (distribution peaks) as functions of log(loading rate), which are plotted in Fig. 4.

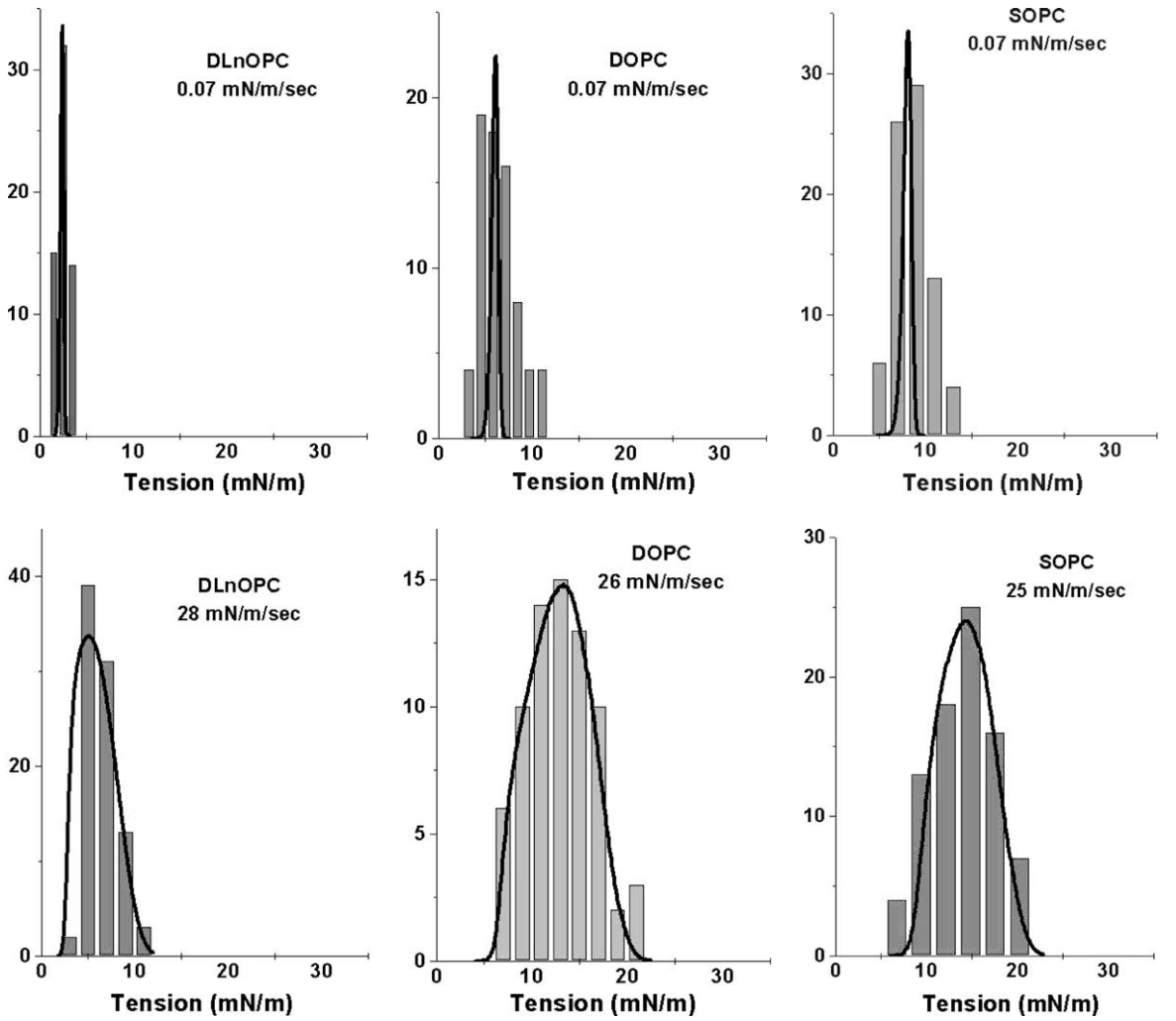

Fig. 3. Histograms of rupture tensions collected at slow and fast loading rates for each type of lipid. Superposed are probability density distributions predicted by the kinetic theory for membrane rupture with the parameters listed in Table 1.

3. Theory and analysis

Reduction in the likelihood of membrane survival with time under stress was appreciated almost a half century ago by Deryagin and Gutop [18]. Extending Zeldovich's [19] classical nucleation theory for cavitation in 3-D liquids, they theorized that the random – but limited – lifetimes of thin fluid films stems from thermally activated nucleation of an unstable hole. In their mesoscopic theory, Deryagin and Gutop used the mechanics of opening a hole in a 2-D continuum to describe the energy landscape governing cavitation. Here, the energy of cohesion is defined by the product of a material edge energy $\boldsymbol{\varepsilon}$ (energy/length) and the hole perimeter $2\pi r$. Under mechanical tension σ, the total energy $E(r)$ is lowered through the potential for mechanical work of expansion, $E(r) \approx (2\pi r)\boldsymbol{\varepsilon} - (\pi r^2)\sigma$, which becomes the dominant term at large radii. A maximum in energy occurs at a *critical radius*, $r_c = \boldsymbol{\varepsilon}/\sigma$, where the height of the *cavitation* barrier is found to be, $E_c = \pi\boldsymbol{\varepsilon}^2/\sigma$. Both height and radial position of the cavitation barrier diminish under tension in the course to rupture. Thus, the thermally-activated frequency for opening an unstable hole (i.e., passage of the cavitation barrier) is expected to rise rapidly under increasing tension over a scale defined and bounded by $\sigma_c = \pi\boldsymbol{\varepsilon}^2/k_B T$.

Subsequently, observations of electrical conductance and transient permeation through solvent-spread membranes [7–11] have revealed that a more complex energy landscape governs dynamics of membrane permeation. In particular, fluctuations of voltage-dependent conductance showed that molecular-scale defects open and close spontaneously in membranes. Initially, these transient structures were imagined to be very small hydrophobic pores that quickly round into hydrophilic structures lined

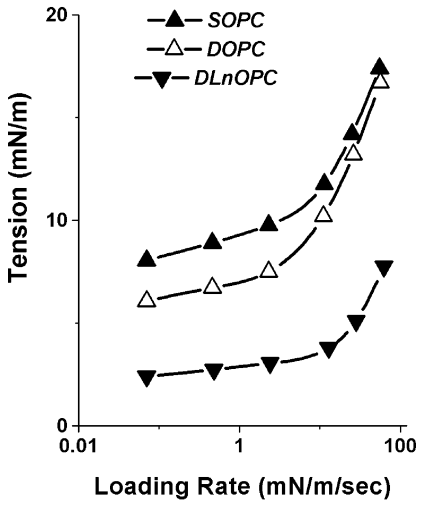

Fig. 4. Dynamic spectra of most frequent rupture tensions (distribution peaks) measured over three orders of magnitude in loading rate. The continuous curves are predictions of the kinetic theory for membrane rupture with the parameters listed in Table 1.

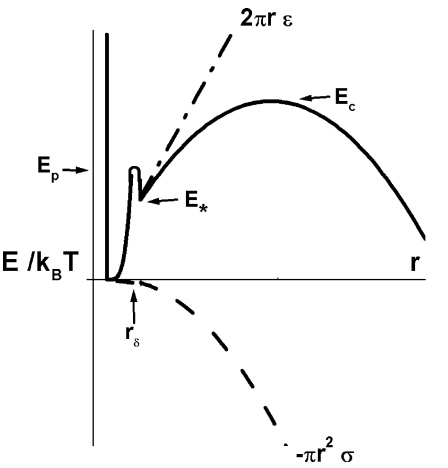

Fig. 5. Schematic illustration of the energy landscape in hole radius space used to model the kinetic process of membrane permeation and rupture. A precursor barrier $E_{\rm p}$ at radius r_δ limits creation/annihilation of a molecular-scale defect, which may then pass the classical cavitation barrier to failure. Beginning from the metastable state at energy $E_\star$, the energy landscape rises to the cavitation barrier set by hole *edge energy* ε and mechanical tension σ, i.e., $E_{\rm c} - E_\star = \pi\varepsilon^2/\sigma$.

with lipid headgroups. Consistent with elastic concepts described earlier by Helfrich [20], continuity of the inner and outer monolayers is expected to diminish the large perimeter energy associated with exposure of hydrocarbon to water and lower the cavitation energy barrier. But perhaps most significant, it was found recently from careful study of transient bursts in membrane conductance that the spikes in conductance represented sequences of nanopore states originating within the lifetime of a closed metastable defect [21]. Moreover, labeled as a pre-pore state, the results implied that no more than one metastable defect was likely to exist in the membrane at any time [21]. Although the molecular-scale structures of such defects and open holes in membranes remain unknown, the electrical conductance measurements have shown clearly that some type of precursor state must be introduced into the classical theory of cavitation. Hence, in the idealized concept of configurations defined by radius space, the energy landscape for open holes would commence from an intermediate state that follows the defect nucleation barrier as schematized in Fig. 5.

3.1. Kinetics of membrane failure

Implicit in the energy landscape sketched in Fig. 5 is the assumption that an unstable hole is linked causally to a particular defect, which is supported by studies of fluctuations in membrane conductance [21]. Thus, although a defect may arise anywhere on the membrane, they remain rare-isolated events that quickly vanish or occasionally evolve to an unstable hole. Easily understood, membrane rupture is most likely to occur when tension rises above the level where the time needed for passage of the cavitation barrier falls to within the lifetime of a defect. Formulated into a hierarchy of master equations that simulates the stochastic process of failure, the model requires analytical prescriptions for each kinetic rate of barrier passage. Beginning with defect formation, we assume that the energy rises steeply from the bound state and is capped by a *sharply-curved* barrier at an energy level of $E_{\rm p}$ defined initially as E_δ in the unstressed state. For a sharp barrier, the height $E_{\rm p}$ will diminish under tension in proportion to the effective area of the defect, i.e., $E_{\rm p}(\sigma) \approx E_\delta - (\pi r_\delta^2)\sigma$. Thus, for a thermally-activated rate of transition $\sim\exp(-E_{\rm p}/k_{\rm B}T)$, the frequency of defect formation $\nu_{0\to\star}$ will grow exponentially on a scale of tension defined by, $\sigma_\delta = k_{\rm B}T/\pi r_\delta^2$, i.e.,

$$\nu_{0\to\star} = \nu_{0\delta}\exp\left(\frac{\sigma}{\sigma_\delta}\right), \tag{1}$$

where the rate prefactor $\nu_{0\delta}$ scales as $\exp(-E_\delta/k_BT)$. Given a sharp defect barrier, the energy $E_\star$ of the metastable state that follows will drop from its initial level E_0 by effectively the same amount under tension, i.e., $E_\star \approx E_0 - (\pi r_\delta^2)\sigma$. Hence, the rate of defect annihilation $\nu_{0\leftarrow\star}$ would remain approximately constant as expressed by

$$\nu_{0\leftarrow\star} \approx \nu_{0\delta} \exp\left(\frac{E_0}{k_BT}\right). \tag{2}$$

Finally, rising from the defect state at energy $E_\star$, the energy landscape is modelled by the mesoscopic mechanics of opening a hole in a continuous material as described above and sketched in Fig. 5. Beyond the *cavitation* barrier defined by, $E_c = E_\star + \pi\varepsilon^2/\sigma$, an unstable hole opens to cause catastrophic failure of the membrane. Scaling barrier height by thermal energy defines the characteristic tension, $\sigma_c = \pi\varepsilon^2/k_BT$, for thermal activation, i.e., rate $\sim\exp(-\sigma_c/\sigma)$. Because the outer barrier is inversely proportional to tension in this mesoscopic model, we see that a defect cannot become an unstable hole at zero tension and that some level of tension is needed to rupture the membrane. As found by Deryagin and Gutop (albeit expressed in a much less organized relation than given here), the frequency of opening an unstable hole $\nu_{\star\rightarrow\text{hole}}$ is predicted to increase dramatically with application of tension up to the level defined by σ_c,

$$\nu_{0\rightarrow\text{hole}} = \nu_{\delta c}\left(\frac{\sigma}{\sigma_c}\right)^{1/2} \exp\left(-\frac{\sigma_c}{\sigma}\right) \quad \{\sigma < \sigma_c\}. \tag{3}$$

The origin (via Zeldovich) of Eq. (3) comes from Kramers' Brownian-dynamics theory [22,23] for thermally-activated escape from a deeply-bound state. Deceptively simple, Kramers' result in the overdamped limit can be summarized by a generic expression for transition (escape) rate, i.e., $\nu_\rightarrow = (D/l_0l_{ts})\exp[-E_b/k_BT]$. Clearly, the major factor is the exponential dependence on height of the barrier E_b, which for cavitation in 2-D is $\exp(-\sigma_c/\sigma)$. The Brownian-*diffusive* dynamics are embodied in an attempt frequency, D/l_0l_{ts}, which is governed by a coefficient ζ ($\equiv k_BT/D$) for damping and the product of two length scales l_0l_{ts}. The length l_0 is defined by the thermal spread in bound state local to the minimum. In the context of hole dynamics, fluctuations in bound state are confined by the perimeter-edge energy and thus the thermal spread is approximated by, $l_0 \approx k_BT/(2\pi\boldsymbol{\varepsilon})$. The length l_{ts} is the energy-weighted width of the transition state. Governed by the fall in energy away from the top of the cavitation barrier, $-\pi(r - r_c)^2\sigma$, the thermal barrier width is estimated by the Gaussian approximation, $l_{ts} \approx (k_BT/\sigma)^{1/2}$. As a consequence of the variable thermal width, the attempt frequency in Eq. (3) is modulated by a weak tension-dependent function $(\sigma/\sigma_c)^{1/2}$. Taken together, these approximations predict that the attempt frequency prefactor $\nu_{\delta c}$ should depend on the ratio of the tension scale to damping factor, $\nu_{\delta c} \approx 2\pi^{1/2}\sigma_c/\zeta$.

Continuing with the perspective of Kramers' theory, it follows that the frequency $\nu_{0\delta}$ for spontaneous nucleation of defects should vary as, $\nu_{0\delta} \sim [k_BT/(\zeta r_\delta^2)]\exp(-E_\delta/k_BT)$, if r_δ^2 is used to approximate the product l_0l_{ts}. As above, the ratio of tension scale to damping factor sets the scale for attempt frequency and we obtain the useful expression, $\nu_{0\delta} \sim (\pi\sigma_\delta/\zeta)\exp(-E_\delta/k_BT)$. Thus, if a common factor ζ characterizes damping of Brownian fluctuations over the entire energy landscape, the attempt frequency $\nu_{\delta c}$ for passage of the cavitation barrier would be directly related to the spontaneous frequency $\nu_{0\delta}$ of defect formation through the height of the defect barrier, i.e., $\nu_{\delta c}/\nu_{0\delta} \approx (\sigma_c/\sigma_\delta)\exp(E_\delta/k_BT)$. Although hypothetical, the assumption of a nearly-constant damping factor is not unreasonable given the very small area compressibility of biomembranes [24]. As such, area changes contributed by defect creation/annihilation and fluctuations in hole size would produce in-plane collective flows at constant surface density. For pure radial flow, membrane surface-shear viscosity η_m determines the damping of circular fluctuations (i.e., $\zeta \approx 4\pi\eta_m$). Completely obscure in this type of mesoscopic model, the frequency scales $\nu_{0\delta}$ and $\nu_{\delta c}$ could involve an area-dependent prefactor often ascribed to the number of sites N_δ for defect formation in a macroscopic membrane. However, as noted above, careful study of fluctuations in membrane conductance indicate that only a single defect state is likely to exist in the membrane at any time [21]. So we neglect the putative factor N_δ which, in any case, merely remains a hidden-homogeneous constant that arbitrarily scales time.

3.2. Dynamic regimes of membrane strength

The hypothesis is that membrane rupture arises from one unstable hole and that this hole must evolve during the lifetime of a particular defect. Hence, with the frequencies defined by Eqs. (1)–(3), the following hierarchy of statistical (Markov) master equations can be used to predict the causal sequence of defect formation and annihilation or evolution to an unstable hole:

$$\begin{aligned}
\frac{dS_0(t)}{dt} &= -\nu_{0\rightarrow\star}S_0(t) + \nu_{0\leftarrow\star}S_\star(t),\\
\frac{dS_\star(t)}{dt} &= -[\nu_{0\leftarrow\star} + \nu_{\star\rightarrow\text{hole}}]S_\star(t) + \nu_{0\rightarrow\star}S_0(t),\\
\frac{dS_{\text{hole}}(t)}{dt} &= \nu_{\star\rightarrow\text{hole}}S_\star(t),
\end{aligned} \tag{4}$$

$S_0(t)$, $S_\star(t)$, and $S_{\rm hole}(t)$ are the probabilities of being in the defect-free *ground state*, metastable state, and ruptured state respectively. The probability density for rupture events in a window of time $t \to t + \Delta t$ is defined by the last equation, $p_{\rm rup}(t) = {\rm d}S_{\rm hole}(t)/{\rm d}t$. Under a ramp of tension $\sigma(t) = \Re_\sigma t$, the distribution of rupture times is transformed by loading rate $\Re_\sigma$ $(=\!{\rm d}\sigma/{\rm d}t)$ into the distribution of rupture tensions, i.e., $p_{\rm rup}(\sigma) = \nu_{\star\to{\rm hole}} S_\star[\sigma(t)]/\Re_\sigma$.

Simple inspection of the energy landscape (Fig. 5) shows that the outer cavitation barrier falls below the defect barrier when tension rises above a level such that $(E_\delta - E_0)/k_{\rm B}T > \sigma_{\rm c}/\sigma$. As a consequence, the model predicts two distinct regimes in the spectrum of rupture tension as a function of loading rate. First, a high strength regime at fast loading rates arises when rupture is limited by creation of a defect. Second, a low strength regime at slow loading rates arises when rupture is limited by hole opening (i.e., passage of the cavitation barrier). In each regime, the statistics of transitions can be approximated by solution to a single Markov equation using one of the following expressions for the limiting transition rate $\nu[\sigma(t)]$, i.e.,

$$\begin{aligned} &\text{defect-limited:} && \nu(\sigma) \approx \nu_{0\delta} \exp\left(\frac{\sigma}{\sigma_\delta}\right), \\ &\text{cavitation-limited:} && \nu(\sigma) \approx \nu_{\delta{\rm c}} \left(\frac{\sigma}{\sigma_{\rm c}}\right)^{1/2} \exp\left(-\frac{\sigma_{\rm c}}{\sigma}\right) \quad \{\sigma < \sigma_{\rm c}\}. \end{aligned} \tag{5}$$

When dominated by passage of a single barrier, the distribution of rupture events in time becomes,

$$p(t) = \nu(t) \exp\left\{-\int\limits_{0\to t} \nu(t')\,{\rm d}t'\right\},$$

and again transformation with the loading rate $\Re_\sigma$ specifies the distribution of rupture tensions,

$$p(\sigma) = \frac{\nu(\sigma)}{r_\sigma} \exp\left\{-\frac{1}{\Re_\sigma}\int\limits_{0\to\sigma} \nu(\sigma')\,{\rm d}\sigma'\right\}.$$

The peak in a tension distribution (most frequent rupture) defines the *rupture strength* $\boldsymbol{\sigma}$ at the particular loading rate $\Re_\sigma$. The dependence of strength $\boldsymbol{\sigma}$ on loading rate is easily derived from the distribution maximum $\partial p/\partial\sigma = 0$, which yields the result, $\nu(\boldsymbol{\sigma}) = \Re_\sigma \{\partial \log(\nu)/\partial\sigma\}_{\sigma=\boldsymbol{\sigma}}$. With this expression and the transition rates in Eqs. (5), the regimes of strength dominated by each barrier are predicted as functions of loading rate:

$$\begin{aligned} &\text{defect-limited:} && \frac{\boldsymbol{\sigma}}{\sigma_\delta} \approx {\rm Log_e}\left(\frac{\Re_\sigma}{\nu_{0\delta}\sigma_\delta}\right), \\ &\text{cavitation-limited:} && -\frac{\sigma_{\rm c}}{\boldsymbol{\sigma}} + {\rm Log_e}\left[\frac{(\boldsymbol{\sigma}/\sigma_{\rm c})^{5/2}}{1+\boldsymbol{\sigma}/2\sigma_{\rm c}}\right] \approx {\rm Log_e}\left(\frac{\Re_\sigma}{\nu_{\delta{\rm c}}\sigma_{\rm c}}\right). \end{aligned} \tag{6}$$

The defect-limited regime is a simple straight line with slope σ_δ, which extrapolates to a loading rate intercept given by, $\Re_\sigma^0 = \nu_{0\delta}\sigma_\delta$. By comparison, the cavitation-limited regime is a shallow-nonlinear curve that rises very slowly as rate increases over many orders of magnitude. The distinctly different shapes of the two limiting regimes result in a prominent crossover in membrane strength when the loading rate is fast enough to rapidly suppress the outer cavitation barrier leaving the defect barrier as the dominant impedance to rupture. As shown next, good estimates of the parameters governing strength can usually be obtained by matching Eqs. (6) to the appropriate portions of an experimental spectrum. However, match of the full solution of the Markov process (Eqs. (4)) to all distributions provides the best quantification of the kinetic parameters and is also needed to place a bound on the metastable state energy E_0.

3.3. Correlation of theory to experiment

Analysis of the membrane rupture experiments begins with matching the strength regimes in Eqs. (6) to the segments of the experimental spectrum that exhibit a shallow-upward curve in strength followed by a linear-like rise over significant spans in loading rate. As shown with the SOPC spectrum in Fig. 6(a), the first step is to match a straight line to the high strength (expected rupture tension) data at fast loading rates >10 mN/m/s. Consistent with the first of Eqs. (6), the outcome is the spontaneous rate for formation of defects $\nu_{0\delta}$ ($\approx$0.18 s^{-1}) and the tension scale $\sigma_\delta = k_{\rm B}T/r_\delta^2$ ($\approx$4 pN) set by defect size. The next step is to match the second of Eqs. (6) for the cavitation-limited regime to the lower values of rupture tension at slow loading rates. As seen in Fig. 6(b), fit of the cavitation-limited regime is much less sensitive to the choice of parameters defined by the edge energy (tension scale $\sigma_{\rm c} = \pi\boldsymbol{\varepsilon}^2/k_{\rm B}T$) and attempt rate $\nu_{\delta{\rm c}}$. When only required to fit the rupture strength at one value, a mere two-fold change of tension scale in a cavitation-limited regime is usually accompanied by many orders of magnitude change in the rate scale (e.g., $\nu_{\delta{\rm c}} \sim 10^3$–$10^{11}$ s^{-1} for $\sigma_{\rm c} \sim$ 80–200 mN/m). However, extending the fit to cover

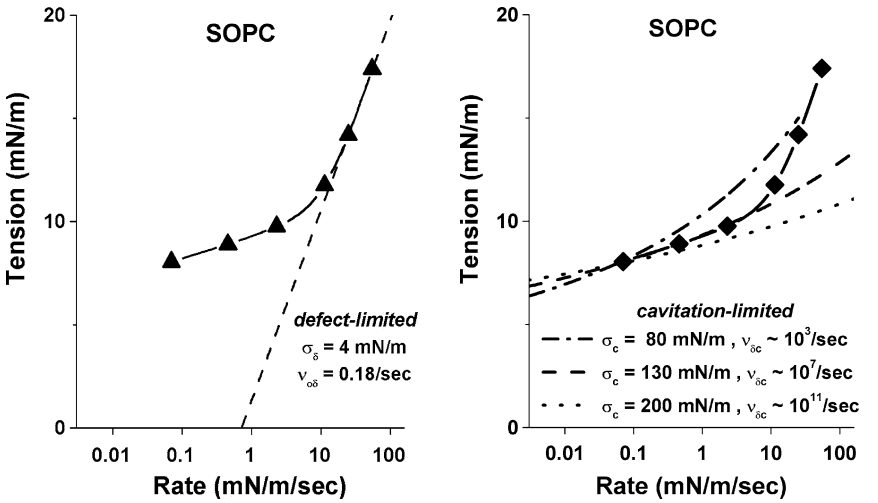

Fig. 6. Left: correlation of the *defect-limited* regime with the dynamic tension spectrum of SOPC vesicles. Right: correlation of the *cavitation-limited* regime with the SOPC spectrum. The solid curve is the full spectrum predicted by solution of the Markov sequence (Eqs. (4)).

Table 1
Material parameters that govern strength of PC membranes

	$\nu_{0\delta}$ (s^{-1})	σ_δ (mN/m)	r_δ (nm)	$\nu_{\delta c}$ (s^{-1})	σ_c (mN/m)	$\boldsymbol{\varepsilon}$ (pJ/m)
DLnOPC	2.0	3.5	0.61	$\sim 1 \times 10^6$	30	6.3
DOPC	0.22	4.0	0.57	$\sim 3.3 \times 10^6$	102	11.5
SOPC	0.18	4.0	0.57	$\sim 5 \times 10^6$	130	13

a large span in loading rate (e.g., 0.07–3 mN/m/s) significantly narrows the range of acceptable values (i.e., $\sigma_c \sim 120$–140 mN/m or $\boldsymbol{\varepsilon} \sim 13 \pm 0.5$ pJ/m and $\nu_{\delta c} \sim 10^6$–10^7 s^{-1}).

Using parameters obtained by the procedure illustrated in Fig. 6 and the Markov equations (4), the final step in data analysis is to refine the values by matching the probability densities for failure to all of the histograms at different loading rates. Examples of tension distributions that result from this procedure are superposed on the histograms in Fig. 3 and the continuous spectra of rupture strength are plotted with the data for most frequent rupture tension in Fig. 4. Here, fits to tension distributions measured in the crossover region from the cavitation-limited to defect-limited regime are particularly useful for restricting the model parameters in difficult cases. The reason is that in the crossover region, the distribution is narrow and rises steeply on the low tension side of the peak but is broadened significantly and falls more gradually on the high tension side. The asymmetry stems from a major difference in kinetic impedance between the two cavitation and defect barriers under tension.

In the final step of fitting probability densities to the measured histograms of tension, the metastable state energy E_0 becomes an additional parameter. Because of the enormous difference in time scales between *cavitation-limited* and *defect-limited* kinetics, dependence on the metastable state energy E_0 was found to be very weak. For instance, in matching all of the distributions for the five lipids, the only clear requirement for optimal fit was that the values of E_0 lie between (0–3)$k_B T$ above the defect-free *ground state*, which was accompanied by a commensurate 10-fold span in the attempt frequency $\nu_{\delta c}$. Hence, the rate of defect annihilation was found to be comparable to the rate of formation (i.e., $\nu_{0 \leftarrow \star} \sim \nu_{0 \rightarrow \star}$). In Table 1, the parameter values are given for the lower bound of $E_0 \sim 0\, k_B T$; at the other bound of $E_0 \sim 3 k_B T$, the only change is that values of $\nu_{\delta c}$ shift upward by an order of magnitude.

4. Conclusions and discussion

For fluid membranes made from diacyl PCs, we find two distinct regimes of rupture strength as a function of dynamic loading. Under very slow ramps of tension, a low strength regime appears where rupture tension increases weakly with ramp rate (i.e., only ~1–2 mN/m over at least two orders of magnitude in rate) and the tension distributions are very narrow. Next, a high strength regime emerges under fast ramps of tension where rupture tension rises dramatically (as much as 10 mN/m for an

order of magnitude increase) and the tension distributions are significantly broadened. Both distribution shape and the functional form of each DTS regime follow directly from a simple kinetic model of the rupture process that begins with nucleation of a nanoscale defect which then either disappears or evolves to an unstable-mesoscopic hole. The model involves five material-dependent parameters. First, defect formation is described by a frequency scale $\nu_{0\delta}$ for spontaneous appearance. Next, the defect energy E_0 in the metastable state sets the frequency scale for annihilation as defined by $\nu_{0\delta}\exp(E_0/k_BT)$. The defect transition is coupled to tension through the area created by a defect, which is described by the apparent defect radius r_δ. Finally, the mesoscale dynamics of hole opening under tension are described by an attempt frequency $\nu_{\delta c}$ and membrane *edge energy* $\boldsymbol{\varepsilon}$, which governs the height of the cavitation barrier relative to the defect state.

As emphasized, somewhat similar concepts arose from the early studies on electrical conductance, transient permeation, and breakdown of solvent-spread membranes where tension remains constant [7,9–11]. However, the most direct evidence for the stochastic events postulated in our model comes from the recent detailed study of fluctuations in membrane conductance under low voltages [21]. In particular, it was found that bursts of transient ∼1 nm holes open and close within the lifetime of a 'pre-pore' defect state [21]. Moreover, it was concluded that the 'pre-pore' defect must be a local-isolated nonconductive state distinct from the closed ground state. Significantly, our DTS experiments imply that nucleation begins with a defect of ∼1 nm cross section and that the defect lifetime ranges from ∼0.1–10 s, which is similar to the survival of the 'pre-pore' state deduced from bursts in electrical activity [21]. Furthermore, the edge energies derived from our experiments (cf. Table 1) are consistent with values of ∼10 pJ/m and 20 pJ/m from the earlier experiments using natural lecithins [9,10,12] as well as ∼10 pJ/m from vesicle electroporation experiments [13] using synthetic C18:0/1 PC. Considering the added complexity of electric fields plus the presence of organic solvent in the case of the BLM experiments, the consistency between parameters obtained from electrical permeation and our mechanical DTS experiments (Table 1) strongly supports the efficacy of the simple kinetic model.

In addition to consistencies with electrical conductance and permeation experiments, correlations of the parameters in Table 1 to other properties of the membranes provide insights into the key determinants of strength. First, although results are only shown here for only three PCs, the edge energies are found to correlate closely with the elastic bending moduli [24], i.e., DLnOPC ($k_c \approx 0.44 \times 10^{-19}$ J), DOPC ($k_c \approx 0.85 \times 10^{-19}$ J), and SOPC ($k_c \approx 0.9 \times 10^{-19}$ J). Increase of edge energy with bending stiffness seems obvious for rounded-hydrophilic edges lined with lipid headgroups. However, much more subtle, the correlation yields a characteristic length $k_c/\boldsymbol{\varepsilon} \approx 7$ nm much larger than the monolayer thickness of ∼2 nm, which would define the curvature of a circular edge. The large value for $k_c/\boldsymbol{\varepsilon}$ seems to imply that the edge shape is flatter than a circular contour. This would require the acyl chains to deviate significantly from the surface normal as if sheared. Moreover, the edge region would include many lipid molecules. Also important but much less precise, the apparent heights of the defect barriers are found to correlate with the membrane-hydrocarbon thicknesses obtained from X-ray diffraction [24]. Estimates of defect barrier height can be calculated from the products of ratios for tension and frequency scales in Table 1, i.e., $\nu_{\delta c}/\nu_0 \approx (\sigma_c/\sigma_\delta)\exp(E_\delta/k_BT)$, again based on the assumption that a common damping coefficient characterizes both defect and hole dynamics. This analysis gives defect barrier energies of $\sim 11k_BT$ for DLnOPC ($h_{ch2} = 2.5$ nm), $\sim 13k_BT$ for DOPC ($h_{ch2} = 2.5$ nm), and $\sim 14k_BT$ for SOPC ($h_{ch2} = 3.1$ nm), which roughly increase at $\sim 4.6k_BT$ nm^{-1} of hydrocarbon thickness [24]. This energy per length is an order of magnitude less than expected for exposure of the acyl chains to water which seems to imply that the defect structure is also bordered by lipid headgroups. Finally, as a corollary to the barrier heights, the ratios $\sigma_c/\nu_{\delta c}$ of tension scale to attempt frequency in Table 1 provide the effective scale for damping of Brownian excitations in lipid membranes given by $\zeta \sim 1 \times 10^{-4}$ mN·s/m.

Acknowledgement

This work was supported by Canadian Institutes for Health Research grant MT7477.

References

[1] E. Evans, D. Needham, J. Phys. Chem. 91 (1987) 4219–4228.
[2] M. Bloom, E. Evans, O.G. Mouritsen, Quart. Rev. Biophys. 24 (1991) 293–397.
[3] D. Needham, R.S. Nunn, Biophys. J. 58 (1990) 997–1009.
[4] F.R. Hallett, J. Marsh, B.G. Nickle, J.M. Wood, Biophys. J. 64 (1993) 435–442.
[5] B.L.-S. Mui, P.R. Cullis, E.A. Evans, T.D. Madden, Biophys. J. 64 (1993) 443–453.
[6] K. Olbrich, W. Rawicz, D. Needham, E. Evans, Biophys. J. 79 (2000) 321–327.
[7] I.G. Abidor, V.B. Arakelyan, L.V. Chernomordik, Y.A. Chizmadzhev, V.F. Pastushenko, M.R. Tarasevich, Bioelectrochem. Bioenerg. 6 (1979) 37–52.
[8] A. Barnett, J. Weaver, Bioelectrochem. Bioenerg. 21 (1991) 163–182.

[9] L.V. Chernomordik, M.M. Kozlov, G.B. Melikyan, I.G. Abidor, V.S. Markin, Y.A. Chizmadzhev, Biochim. Biophys. Acta 812 (1985) 643–655.
[10] L.V. Chernomordik, S.I. Sukharev, S.V. Popov, V.F. Pastushenko, A.V. Sokirko, I.G. Abidor, Y.A. Chizmadzhev, Biochim. Biophys. Acta 902 (1987) 360–373.
[11] R.W. Glaser, S.L. Leikin, L.V. Chernomordik, V.F. Pastushenko, A.I. Sokirko, Biochim. Biophys. Acta 940 (1988) 275–287.
[12] W. Harbich, W. Helfrich, Z. Naturforsch. Teil A 34 (1979) 1063–1065.
[13] D.V. Zhelev, D. Needham, Biochim. Biophys. Acta 1147 (1993) 89–104.
[14] O. Sandre, L. Moreaux, F. Brochard-Wyart, Proc. Nat. Acad. Sci. USA 96 (1999) 10591–10596.
[15] F. Brochard-Wyart, P.G. de Gennes, O. Sandre, Physica A 278 (2000) 32–51.
[16] D. Needham, T.J. McIntosh, E. Evans, Biochem. 27 (1988) 4668–4673.
[17] R. Kwok, E. Evans, Biophys. J. 35 (1981) 637–652.
[18] B.V. Deryagin, Y.V. Gutop, Kolloidn. Zh. 24 (1962) 370–374.
[19] J.B. Zeldovich, Acta Physicochim. URSS 18 (1943) 1–22.
[20] W. Helfrich, Phys. Lett. A 50 (1974) 115–116.
[21] K.C. Melikov, V.A. Frolov, A. Shcherbakov, A.V. Samsonov, Y.A. Chizmadzhev, L.V. Chernomordik, Biophys. J. 80 (2001) 1829–1836.
[22] H.A. Kramers, Physica (Utrecht) 7 (1940) 284–304.
[23] P. Hanggi, P. Talkner, M. Borkovec, Rev. Mod. Phys. 62 (1990) 251–342.
[24] W. Rawicz, K. Olbrich, T. McIntosh, D. Needham, E. Evans, Biophys. J. 79 (2000) 328–339.